The EMBO Journal (2012) 31, 3411–3421 | © 2012 European Molecular Biology Organization | Some Rights Reserved 0261-4189/12
www.embojournal.org

THE EMBO JOURNAL

EMBO open

Alternating access mechanism in the POT family of oligopeptide transporters

Nicolae Solcan[1,2], Jane Kwok[1], Philip W Fowler[1], Alexander D Cameron[2,3,4], David Drew[4], So Iwata[2,3,4,5,6] and Simon Newstead[1,2,3,*]

[1]Department of Biochemistry, University of Oxford, Oxford, UK, [2]Membrane Protein Laboratory, Diamond Light Source, Harwell Science and Innovation Campus, Didcot, UK, [3]Research Complex at Harwell, Rutherford Appleton Laboratory, Didcot, UK, [4]Division of Molecular Biosciences, Imperial College London, London, UK, [5]Japan Science and Technology Agency, ERATO Human Receptor Crystallography Project, Kyoto, Japan and [6]Department of Cell Biology, Graduate School of Medicine, Kyoto University, Kyoto, Japan

Short chain peptides are actively transported across membranes as an efficient route for dietary protein absorption and for maintaining cellular homeostasis. In mammals, peptide transport occurs via PepT1 and PepT2, which belong to the proton-dependent oligopeptide transporter, or POT family. The recent crystal structure of a bacterial POT transporter confirmed that they belong to the major facilitator superfamily of secondary active transporters. Despite the functional characterization of POT family members in bacteria, fungi and mammals, a detailed model for peptide recognition and transport remains unavailable. In this study, we report the 3.3-Å resolution crystal structure and functional characterization of a POT family transporter from the bacterium *Streptococcus thermophilus*. Crystallized in an inward open conformation the structure identifies a hinge-like movement within the C-terminal half of the transporter that facilitates opening of an intracellular gate controlling access to a central peptide-binding site. Our associated functional data support a model for peptide transport that highlights the importance of salt bridge interactions in orchestrating alternating access within the POT family.

The EMBO Journal (2012) **31,** 3411–3421. doi:10.1038/emboj.2012.157; Published online 1 June 2012
Subject Categories: membranes & transport; structural biology
Keywords: alternating access mechanism; major facilitator superfamily; peptide transport; PepT1; POT family

Introduction

Peptide transport is the main route through which the body absorbs and retains dietary protein and as such plays an important role in human physiology (Steinhardt and Adibi, 1986; Matthews, 1991). Ingested protein is absorbed across the intestinal brush border membrane in the form of di- and tri-peptides through the action of the integral membrane peptide transporter, PepT1 (Fei *et al*, 1994; Liang *et al*, 1995; Leibach and Ganapathy, 1996). A similar process occurs at the renal epithelium, where PepT2 re-absorbs small peptides from the glomerular filtrate (Daniel and Rubio-Aliaga, 2003; Biegel *et al*, 2006). Both PepT1 and PepT2 recognize a diverse library of peptide substrates, which include most proteinogenic di- and tri-peptides (Matthews, 1975), in keeping with their function as major nutrient transporters. They also recognize and play an active role in the oral absorption and renal retention of many drug compounds with a steric resemblance to peptides, which include the commonly prescribed β-lactam antibiotics (Luckner and Brandsch, 2005; Anderson and Thwaites, 2010). A detailed understanding of the structure, transport mechanism and conformational changes of PepT1 and PepT2 would therefore substantially improve efforts to utilize these transporters for improved drug delivery, distribution and retention (Brandsch, 2009).

PepT1 and PepT2 belong to the solute carrier (SLC) 15 gene family and phylogenetically form part of the much larger proton-dependent oligopeptide transporter, or POT family (TC 2.A.17) that is widely distributed within prokaryotes and eukaryotes (Daniel *et al*, 2006). They are all proton (H^+)-driven symporters, using the inwardly direct proton electrochemical gradient ($\Delta\mu_{H+}$) to drive the uptake of peptides across cell membranes (Daniel and Kottra, 2004). The high degree of sequence conservation between prokaryotic and eukaryotic members (Supplementary Figure S1) indicates that they operate through a conserved mechanism (Daniel *et al*, 2006). This conclusion is supported by several biochemical studies on prokaryotic PepT1 and PepT2 homologues (Fang *et al*, 2000; Weitz *et al*, 2007; Harder *et al*, 2008; Ernst *et al*, 2009; Jensen *et al*, 2011; Malle *et al*, 2011).

Structurally, the POT family sits within the larger and functionally diverse major facilitator superfamily (MFS) of secondary active transporters (Pao *et al*, 1998) that typically contain 12, but sometimes 14, trans-membrane (TM) helices. Crystal structures from several MFS transporters reveal a common fold consisting of two 6-TM bundles that assemble together in the membrane to form a 'V'-shaped transporter with a central substrate-binding site formed between the two bundles (Hirai *et al*, 2002; Abramson *et al*, 2003; Huang *et al*, 2003; Yin *et al*, 2006; Dang *et al*, 2010). Based on these structures and numerous biophysical studies on LacY, the lactose permease from *Escherichia coli* (Smirnova *et al*, 2011), a general model of transport within the MFS has been proposed. This broadly describes transport occurring through the movement of each bundle around a central binding site and is commonly referred to as the rocking bundle mechanism (Law *et al*, 2008). Recently, the first crystal structure of a POT transporter, $PepT_{So}$, was determined (Newstead *et al*, 2011), revealing a novel asymmetrical occluded conformation, previously unobserved for this class of

*Corresponding author. Department of Biochemistry, University of Oxford, South Parks Road, Oxford OX1 3QU, UK.
Tel.: +44 1865 613319; Fax: +44 1865 613201;
E-mail: simon.newstead@bioch.ox.ac.uk

Received: 22 February 2012; accepted: 3 May 2012; published online: 1 June 2012

transporter. An intracellular gate that appears to be conserved among many POT family members was observed restricting the exit of a bound ligand from the intracellular side of the transporter. The structure and mechanism of these gates within the general rocking bundle model of transport is currently not well defined for the MFS, largely due to the absence of crystal structures representing different stages of the transport cycle from the same family. Here, we report the crystal structure of a second POT family transporter from the bacterium *Streptococcus thermophilus*, $PepT_{St}$ refined at 3.3 Å resolution. In contrast to the occluded structure of $PepT_{So}$, the structure of $PepT_{St}$ reveals an inward facing conformation that provides significant new insight into the release mechanism of the intracellular gate and the role of conserved salt bridge interactions in orchestrating structural changes during transport. We further identify key residues involved in proton binding and regulating peptide affinity within the binding site, which combined with the structural data provide a more detailed structural model for peptide transport within the POT family.

Results

Structure, kinetics and substrate specificity of $PepT_{St}$

The structure of $PepT_{St}$ was solved using multiple isomorphous replacement with anomalous scattering (MIRAS) using mercury derivatized crystals and seleno-L-methionine incorporated protein (for further details, see Supplementary data). The structure was refined at 3.3 Å resolution to a final R_{factor} of 27.3% and R_{free} of 28.9% (Table I). $PepT_{St}$ adopts the canonical MFS fold with helices H1–H6 forming the N-terminal bundle and helices H7–H12 the C-terminal bundle and represents an inward facing conformation for the POT family (Figure 1A). The two bundles adopt similar structures and superimpose with a root mean square deviation (r.m.s.d.) of 2.7 Å over 153 Cα atoms. The peptide-binding site is located at the apex of an elongated hydrophilic cavity that opens outwards from the interior towards the intracellular side of the membrane (Figure 1B). The cavity has overall dimensions of ~14 Å × 13 Å × 20 Å. The extracellular side of the binding site by comparison is tightly sealed, through the close packing of helices H1 and H2 against H7 and H8 forming an occlusion that hereafter we refer to as the extracellular gate. In addition to the two 6-TM bundles, $PepT_{St}$ contains two other helices, HA and HB, which are inserted within the intracellular loop connecting helices H6 and H7 and pack to one side of the transporter (Supplementary Figure S3). Similar helices were observed in the related POT family member, $PepT_{So}$ (Newstead *et al*, 2011). The absence of these helices in the fungal, plant and metazoan protein sequences suggests that they do not form part of a conserved transport mechanism and short 100 ns atomistic simulations indicate that these helices move semi-independently from the 'core' 12 TM MFS fold (Supplementary Figure S4).

To establish $PepT_{St}$ as a model for understanding transport within the wider POT family, purified protein was reconstituted into a proton-driven proteoliposome system (for further details, see Supplementary data). Maximal transport of the peptide analogue glycylsarcosine was observed at pH 6.5 with an apparent affinity constant, K_M^{app}, of 9.3 mM and a maximal rate of uptake, V_{max}, of 631 nmol min^{-1} mg^{-1} $PepT_{St}$ (Supplementary Figure S5), consistent with the values obtained for DtpT from *Lactococcus lactis* using a similar assay technique (Fang *et al*, 2000). The size and charge preference for peptides was also investigated (Figure 1C). As observed for the mammalian PepT1 protein (Fei *et al*,

Table I Data collection, phasing and refinement statistics for $PepT_{St}$

	Native (high)	Native (low)	MMC-1[a]	MMC-2	Se
Data collection					
Space group	$P2_12_12_1$	$P2_12_12_1$	$P2_12_12_1$	$P2_12_12_1$	$P2_12_12_1$
Cell dimensions					
a, *b*, *c* (Å)	89.6, 113.1, 215.3	90.4, 113.6, 223.4	90.7, 113.8, 222.5	90.7, 113.7, 224.9	90.6, 113.6, 222.61
α, β, γ (deg)	90, 90, 90	90, 90, 90	90, 90, 90	90, 90, 90	90, 90, 90
Resolution (Å)	107–3.3 (3.4–3.3)	74–4.0 (4.1–4.0)	70–4.5 (4.6–4.5)	70–5.9 (6.0–5.9)	90–4.5 (4.6–4.5)
R_{merge}[b]	10.1 (111.2)	8.1 (85.0)	9.4 (82.2)	6.4 (60.3)	6.6 (47.9)
$I/\sigma I$	5.1 (1.1)	9.6 (1.9)	10.9 (2.7)	16.8 (2.0)	9.0 (2.7)
Completeness (%)	99.3 (99.9)	94.0 (97.4)	97.2 (96.2)	98.5 (93.6)	96.8 (90.9)
Redundancy	3.5 (3.5)	3.0 (3.0)	6.7 (6.5)	6.8 (6.9)	3.5 (3.5)
R_{cullis} (%)			90.3/95.3	109.2/93.5	94.6/90.8
Isomorphous/anomalous Phasing power[c]			0.583/0.459	0.345/0.709	0.658/0.646
Isomorphous/anomalous					
Refinement					
Resolution (Å)	29–3.3				
No. of reflections	27 943				
R_{work}/R_{free}	27.3/28.9				
No. of atoms	13 898				
Protein					
r.m.s.d.					
Bond lengths (Å)	0.01				
Bond angles (deg)	0.98				

[a]For details on derivatization, see Supplementary data.
[b]The last shell R_{merge} is high for some of the derivative data due to severe anisotropy in the diffraction images.
[c]Phasing power = rms ($|F_H|/((F_H + F_P) - (F_{PH}))$).

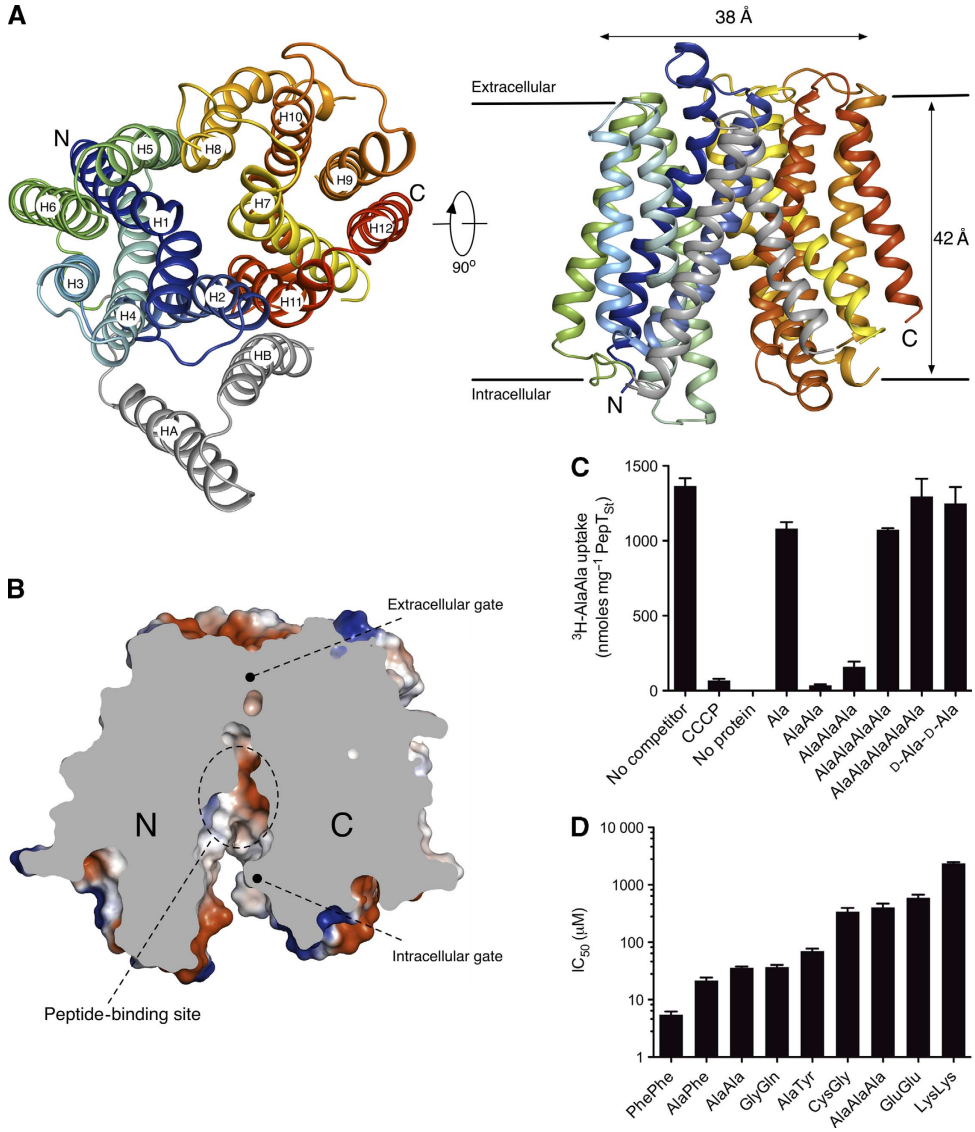

Figure 1 PepT$_{St}$ structure reveals an inward open conformation. (**A**) Overall structure of PepT$_{St}$ viewed from the extracellular side of the molecule. The 12-TM MFS fold is coloured blue to red with helices HA and HB coloured grey. The helices are labelled. The right-hand image shows a view in the plane of membrane with approximate dimensions of the molecule. (**B**) Slab through the surface electrostatic potential of PepT$_{St}$ viewed in the plane of membrane to highlight the extracellular gate, central peptide-binding site and intracellular gate. (**C**) Peptide transport by PepT$_{St}$ is driven by an inwardly directed proton gradient and selective for L di- and tri-peptides. 'No competitor' refers to the condition where only ^{3}H di-alanine peptide was present in the external buffer, without additional cold peptides. 'No protein' refers to empty liposomes. 'CCCP' refers to addition of the proton ionophore carbonyl cyanide *m*-chlorophenyl hydrazine to the external buffer. Error bars indicate the standard deviations from triplicate experiments. (**D**) PepT$_{St}$ displays higher affinity for hydrophobic di-peptides and can discriminate based on peptide size and charge.

1994), only di- and tri-peptides competed effectively for uptake of the ^{3}H di-alanine reporter peptide, with an approximate 10-fold increase in affinity for di-alanine (IC_{50} 0.03 ± 0.01 mM) over that for tri-alanine (0.4 ± 0.05 mM; Figure 1D). The affinity for hydrophobic di-peptides is higher than for charged di-peptides, ranging from 0.05 ± 0.01 mM for di-phenylalanine to 2 ± 0.2 mM for di-lysine. Di-glutamate competes as well for uptake as tri-alanine, suggesting that the peptide-binding site effectively discriminates between positive and negatively charged side chains, which is also the case for the mammalian homologues (Eddy *et al*, 1995). Also consistent with mammalian peptide transporters, transport by PepT$_{St}$ appears to be stereospecific, with no discernable inhibition by D-Ala-D-Ala.

The extracellular gate is stabilized by conserved salt bridge interactions

Alternating access within many secondary active transporters occurs through conformational changes that result in the ligand binding sites being alternatively exposed to either side of the membrane. These changes are often described in terms of the opening and closing of gates, which are often local areas of the structure that move in response to ligand or ion binding (reviewed in Forrest *et al*, 2011). Access to the peptide-binding site from the extracellular side of the membrane in PepT$_{St}$ will require a substantial conformational change within the extracellular gate. Two salt bridge interactions can be identified that facilitate the close packing of the gate helices in the structure (Figure 2A),

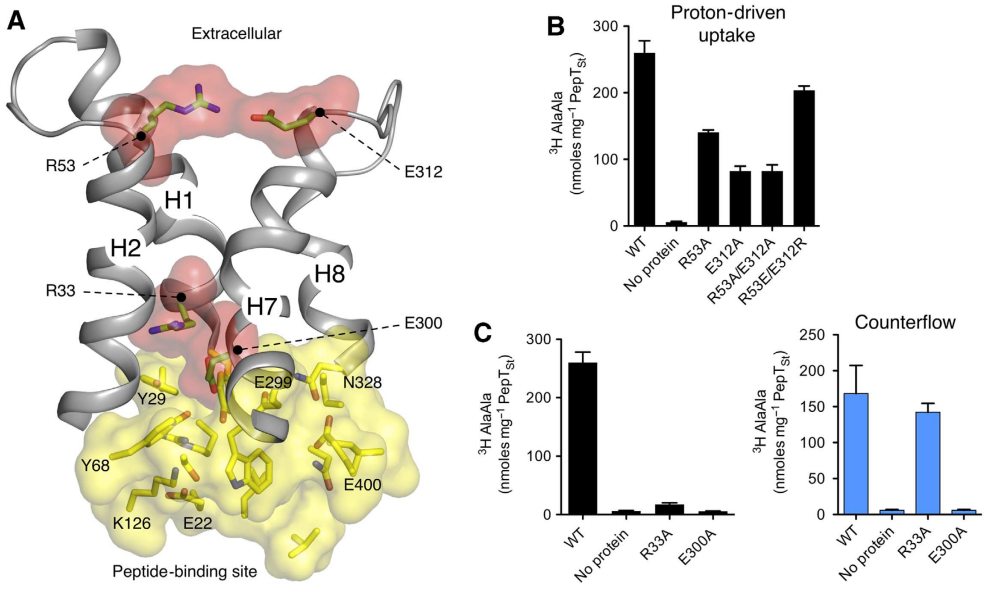

Figure 2 Salt bridges facilitate closure of the extracellular gate. (**A**) Two prominent salt bridge interactions (Arg53–Glu312: distance ~2.9 Å and Arg33–Glu300: distance ~3.8 Å) are observed facilitating the close packing between helix hairpins H1–H2 and H7–H8 in the extracellular gate. Residues forming the central peptide-binding site are shown in yellow and the salt bride interactions in red. Helices and residues are labelled. (**B**) Effect of mutations in the Arg53–Glu312 salt bridge on proton-driven ^{3}H di-alanine uptake. (**C**) Effect of mutations in the Arg33 and Glu300 salt bridge on proton driven (left-black bars) and peptide-driven counterflow transport (right-blue bars). Details of the counterflow experiments can be found in Supplementary data. Error bars indicate the standard deviations from triplicate experiments.

namely Arg53 (H1) with Glu312 (H7) and Arg33 (H1) with Glu300 (H7). The Arg53–Glu312 salt bridge is distal from the peptide-binding site, being located at the extracellular side of the transporter. Mutation of Arg53 to alanine reduced the proton-driven uptake of di-alanine by 50% compared with the WT protein, whereas a similar mutation of Glu312 reduced uptake by 70%, similar to a double alanine mutant (Figure 2B); however, a charge swapped mutant only showed a 20% reduction in transport. Taken together, these results suggest the Arg53–Glu312 salt bridge plays a supportive rather than essential role during transport. In contrast, alanine mutations at the second salt bridge, between Arg33 and Glu300, that is positioned next to the peptide-binding site had a substantial effect on transport. The mutation of Glu300 to alanine abolished uptake in both the proton-driven and peptide-driven counterflow assay, whereas transport in the Arg33 mutant was only abolished in the proton-driven assay (Figure 2C). This is an intriguing result, indicating that Arg33 is important for coupling peptide transport to the inwardly directed proton gradient whereas Glu300 appears to affect peptide recognition and/or structural movements during transport; this role is consistent with the prominent position of Glu300 within the extracellular gate. However, an additional role for Glu300 in proton coupling should not be disregarded, as this may be required for subsequent peptide binding, a situation that would give similar results to those observed. Nevertheless, as discussed below, we propose these interactions are important in orchestrating alternating access within the POT family.

Residues involved in proton binding and the role of the ExxERFxYY motif

Contributing to the central cavity is a conserved sequence motif (ExxERFxYY) on helix H1 that is found in all POT family members studied to date (Supplementary Figure S1; Daniel *et al*, 2006). The functional significance of this motif however remains ambiguous. The arginine and tyrosine residues from this motif are positioned close to the ligand seen in the binding pocket of the occluded structure of PepT$_{So}$ (Newstead *et al*, 2011). To address the functional role of this motif in PepT$_{St}$, Glu22, Glu25, Arg26, Tyr29 and Ty30 (Figure 3A) were mutated sequentially to alanine (Supplementary Table 1); however, as the Arg26Ala mutant did not express this was further substituted for lysine. We interpret our data to indicate the ExxERFxYY motif is important for proton binding during transport, as the alanine mutants showed measurable uptake only under counterflow conditions (Figure 3B and C). The exception was Tyr29, which retained 75% of WT levels and as shown below is likely to function in determining peptide specificity.

In the structure, Glu25 and Arg26 interact through a salt bridge at a distance of 2.5–2.8 Å, which is positioned close ~3.2 Å to Glu22 on helix H1 (Figure 3A; Supplementary Figure S2A). To test the functional significance of this salt bridge, we substituted Glu22 and Glu25 to glutamine. As with the alanine substitutions described above, both Glu22Gln and Glu25Gln variants were inactive under proton-driven uptake (Figure 3B) but retained activity under counterflow (Figure 3C), providing further support for a role in the proton coupling mechanism and suggesting that the chemistry of the salt bridge between Glu25 and Arg26 is an important component of the ExxERFxYY motif in PepT$_{St}$. Positioned close ~3.8 Å to Arg26 in the peptide-binding site is a conserved lysine on helix H4, Lys126 (Figure 3A). Lys126 is absolutely conserved throughout the POT family (Supplementary Figure S1) and holds a prominent position within the binding sites of both PepT$_{St}$ and PepT$_{So}$ (Newstead *et al*, 2011). Mutation of Lys126 to alanine only abolished proton-driven uptake

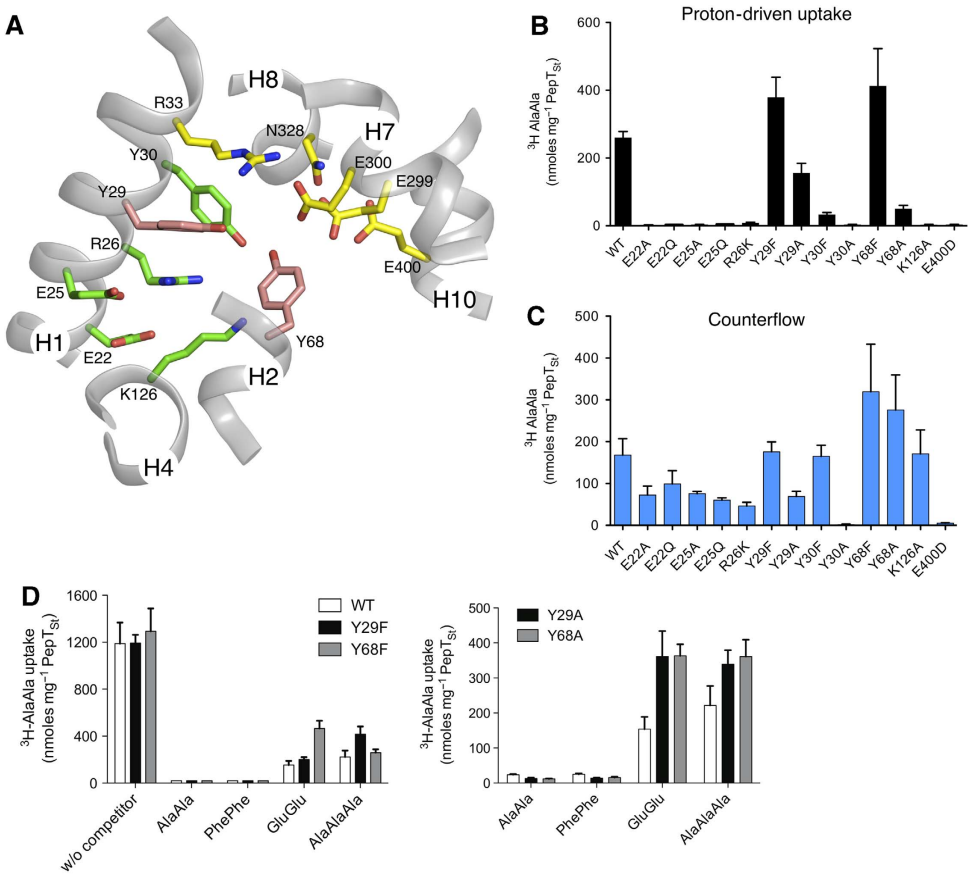

E

IC_{50} (mM)	WT	Y29F	Y68F
Glu-Glu	0.56 ± 0.07	0.48 ± 0.05	1.63 ± 0.09
Phe-Phe	0.005 ± 0.002	0.006 ± 0.004	0.02 ± 0.002
Ala-Ala	0.36 ± 0.02	0.50 ± 0.06	0.51 ± 0.05
Ala-Ala-Ala	0.40 ± 0.06	1.40 ± 0.02	0.35 ± 0.003

Figure 3 Proton binding and peptide specificity reside predominantly within the N-terminal domain of $PepT_{St}$. (**A**) Peptide-binding site as viewed from the plane of the membrane showing the ExxERFxYY motif on helix H1. Residues are coloured according to their predicted role, with proton binding (green), peptide specificity (pink) and transport (yellow). (**B**) Effect of substitutions within the peptide-binding site on proton-driven uptake. (**C**) Effect of equivalent substitutions on peptide driven counterflow uptake. (**D**) Effect of phenylalanine and alanine substitutions at Tyr29 and Tyr68 on the ability of different L-isomer peptides to compete for uptake of di-alanine in proton-driven uptake. (**E**) Change in IC_{50} values upon substitution of Tyr29 and Tyr68 to phenylalanine. The IC_{50} values for the different peptides were calculated as described in Supplementary data. Error bars indicate the standard deviations from triplicate experiments.

(Figure 3B and C), providing strong evidence for proton binding during transport. Interestingly, the primary amine group is absolutely required as substitution for arginine, histidine or glutamine all abolished proton-driven uptake, but left counterflow unaffected (Supplementary Figure S6). The close positioning of Lys126 to the ExxERFxYY motif in the structure suggests that a functional interaction during transport is possible, potentially acting to regulate the proton coupling we observe.

Another striking feature of the central cavity is the cluster of three glutamates on the C-terminal half of the molecule (Figure 3A). Glutamates are likely candidates for proton binding and suggested to play such a role in the fucose and lactose permeases (Dang *et al*, 2010; Kaback *et al*, 2011). Two of the glutamates in $PepT_{St}$, Glu299 and Glu300 are found on H7, with Glu300 forming part of the extracellular gate, as discussed above. Substitution of Glu299 to alanine, glutamine or the conservative aspartic acid resulted in a protein too unstable to be produced (Supplementary Table 1). Although an acidic residue is highly conserved at the equivalent position to Glu300 on H7, the preceding residue is often either phenylalanine or tyrosine (Supplementary Figure S1), suggesting that Glu299 is playing a structural or stabilizing role unique to $PepT_{St}$. The third glutamate, Glu400, is situated on H11 and close ~3.2 Å to a conserved asparagine on H8, Asn328. Of these glutamates, only Glu400 is strictly conserved within the POT family. The equivalent glutamate to Glu400 in human PepT1 (Glu595) is attributed to binding the N-terminus of peptide substrates (Meredith *et al*, 2000), a role supported in biochemical studies on the *E. coli* peptide transporter, YjdL (Jensen *et al*, 2011). In $PepT_{St}$, the Glu400Ala mutation failed to express; similar mutations in

human PepT1 and YjdL express but were not functional (Bolger *et al*, 1998; Jensen *et al*, 2011). Surprisingly, the conservative Glu400Asp mutation also abolished proton-driven and counterflow uptake (Figure 3C), indicating a requirement for the increased length of the glutamate side chain in $PepT_{St}$.

Role of conserved tyrosine's in determining peptide binding affinities

The peptide-binding site contains three prominent tyrosine side chains, Tyr29 and Tyr30, contributed from helix H1, and Tyr68 from helix H2 (Figure 3A). A similar cluster of tyrosine side chains was observed in the binding site of $PepT_{So}$ (Newstead *et al*, 2011) and suggested to play a role in mediating peptide specificity, as shown for rabbit PepT1 (Pieri *et al*, 2009). The hydroxyl groups of both Tyr29 and Tyr68 do not contribute to proton binding, as their mutation to phenylalanine had little impact on proton-driven uptake compared with WT (Figure 3B). The Tyr29Ala mutant did show reduced uptake in counterflow, however, demonstrating that the ExxERFxYY motif has additional roles to proton binding during transport. To investigate the function of Tyr29 and Tyr68 further we carried out a series of competition experiments with a library of di- and tri-peptides (Figure 3D). The phenyalanine mutants showed distinct changes in their affinity for di-Glu and tri-Ala peptides compared with the WT protein, with the alanine mutants losing their ability to transport these peptides altogether while still retaining affinity for di-Phe and di-Ala peptides (Figure 3D). This difference in the observed affinity between peptides, in particular for the alanine mutations, suggests that Tyr29 and Tyr68 are important in determining peptide affinity. To quantify the contribution made by Tyr29 and Tyr68 to peptide affinity, IC_{50} values for these peptides were calculated for each of the phenylalanine mutants (Figure 3E). The Tyr29Phe mutant had a decreased affinity for tri-alanine, IC_{50} of 1.4 mM compared with 0.4 mM for the WT, while still retaining WT affinity levels for di-Glu. The Tyr68Phe mutant displays a decreased affinity for di-Glu, IC_{50} values of 1.63 mM compared with 0.56 mM for the WT protein while retaining the same affinity for tri-alanine. Taken together, these results identify helices H1 and H2 within the $PepT_{St}$ as critical sites of interaction with the peptide during transport.

Comparison between inward open and occluded POT family transporters reveals a structural movement that opens the intracellular gate

Comparing $PepT_{St}$ and $PepT_{So}$, helices H1–H6 superimpose with an r.m.s.d. of 1.6 Å for 167 Cα atoms, adopting a similar arrangement between the two structures (Supplementary Figures S1 and S7). The main difference occurs within the C-terminal bundle, where helices H7–H12 superimpose with an r.m.s.d. of 2.3 Å for 127 Cα atoms. In the occluded structure of $PepT_{So}$, an intracellular gate constructed from conserved side chain interactions between helices H4–H5 and H10–H11 prevents the bound ligand from exiting the binding site (Newstead *et al*, 2011). Comparison with the inward open structure of $PepT_{St}$ shows the cytoplasmic halves of H7, H10 and H11 swing away from helices H4–H5 resulting in the release of this gate, opening the peptide-binding site to the intracellular side of the membrane (Figure 4A). Unexpectedly, opening of this gate does not require movement of the entire H10–H11 helix hairpin, as previously conjectured (Newstead *et al*, 2011), but appears to be localized towards the cytoplasmic halves of these helices and consist of a hinge like movement at the apex of the H10–H11 hairpin (Figure 4A). Specifically, the gate opens due to bending at Gly407 and Trp427 on helices H10 and H11, respectively. This results in the intracellular ends of these helices moving ~13 Å away from their respective positions in the occluded conformation. This movement appears coordinated with respect to helix H7, which straightens in $PepT_{St}$ providing space for H10 and H11 to move. Gly407 and Trp427 are located at the same point within the H10–H11 helix hairpin, effectively forming a hinge or pivot point, which would control whether the intracellular gate is open or closed between the occluded and inward facing conformation. Indeed, substitution of either Gly407 or Trp427 to alanine abolished both proton-driven and counterflow uptake (Figure 4B). A Trp427Phe substitution however did not adversely affect transport in either assay, implying a bulky hydrophobic residue at this position is sufficient for normal functioning of the gate. Of note is that glycine residues are found at equivalent positions to Gly407 in GlpT (Lemieux *et al*, 2004), FucP (Dang *et al*, 2010), EmrD (Yin *et al*, 2006) and LacY (Abramson *et al*, 2003), implying a wider significance for flexibility within helices H10 and H11 within the MFS. A further localized movement is observed at the extracellular end of H11, at another conserved glycine, Gly434. This movement results in closer packing of helix H11 with H2 and H7 and would result in the closure of the extracellular cavity observed in the occluded $PepT_{So}$ structure upon adoption of the inward open state.

Discussion

A model for proton-driven peptide symport within the POT family

Considering proton coupled peptide symport within the POT family, a picture emerges from our study whereby substitutions of conserved residues in the N-terminal domain affect aspects of both proton binding and peptide specificity. Our mutagenesis data for $PepT_{St}$ are consistent with analogous studies on PepT1 and PepT2, which concluded the N-terminal helices dictated peptide binding and affinity characteristics (Döring *et al*, 1996, 2002; Fei *et al*, 1998). Structural comparison of the inward facing $PepT_{St}$ structure with the occluded conformation of $PepT_{So}$ supports our previous model where we proposed the C-terminal domain is more dynamic, with helices H10 and H11 facilitating opening of the central peptide-binding site to the interior of the cell during transport. An important role for salt bridge interactions was also evident from our study, where they appear prominently within the extracellular side of the transporter and within the conserved ExxERFxYY motif in helix H1.

On the basis of both the structural and biochemical analyses, we add further mechanistic details to our earlier structural model of peptide transport (Newstead *et al*, 2011) that we have summarized in Figure 5. The model employs alternating salt bridge interactions at both the extracellular and intracellular ends of the peptide-binding site that form and break during transport. In the outward facing conformation (Figure 5A), the central binding site should be accessible to the extracellular side of the membrane to receive peptides,

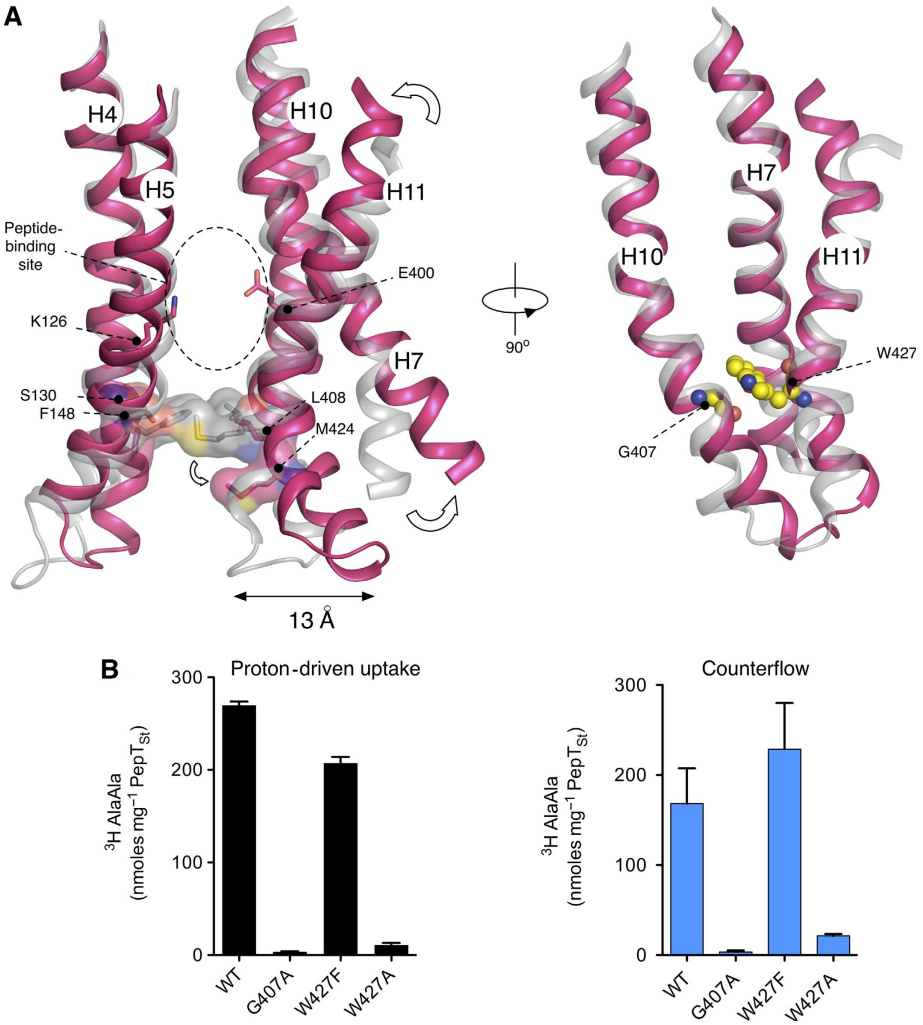

Figure 4 The intracellular gate is controlled through localized hinge bending in helices H10 and H11. (**A**) Comparison between the inward open $PepT_{St}$ (magenta) and occluded $PepT_{So}$ structure (grey) (PDB 2XUT) with arrows showing the hinge-like movement that opens the intracellular gate. View is from the membrane plane. The intracellular gate is shown in the occluded ($PepT_{So}$) and open ($PepT_{St}$) states. Residue numbers are for $PepT_{St}$. The peptide-binding site containing Lys126 and Glu400 is indicated. Right, view rotated 90° showing the Gly407 and Trp427 as spheres and their position within the helices. (**B**) Effect of mutating the hinge residues on proton driven (left-black bars) and peptide-driven counterflow uptake (right-blue bars) in $PepT_{St}$. Error bars indicate the standard deviations from triplicate experiments.

in a conformation potentially resembling that of the fucose permease FucP (Dang *et al*, 2010). Conserved side chains involved in proton binding should be accessible, as proton binding is predicted to occur before recognition of peptide (Sala-Rabanal *et al*, 2008). Our study suggests that protonation is likely within the N-terminal domain involving residues from the ExxERFxYY motif on helix H1 with an important role for Lys126 on helix H4. Interestingly, a superposition of both N- and C-terminal bundles of $PepT_{St}$ onto those of the proton coupled fucose transporter, FucP (Supplementary Figure S8) places Lys126 in the same position as a conserved glutamate, Glu135 in FucP which upon protonation is predicted to trigger the switch to the inward facing state (Dang *et al*, 2010). Similarly, in superimposing the respective C-terminal domains, Glu400 of $PepT_{St}$, which our data suggest is involved in structural aspects of peptide transport, is close to Tyr365 in FucP, which is the proposed interaction partner of Glu135. A speculative function for Lys126 may therefore be to form a salt bridge with Glu400 in the outward open conformation, facilitating the closer packing of helices H4 and H10 and sealing the binding site to the interior of the cell in the outward facing state.

Following proton binding, entry of either a di- or tri-peptide into the central cavity should facilitate closure of the extracellular gate to occlude the peptide within the binding site (Figure 5B). Studies in LacY suggest that residues from both 6-TM bundles act to coordinate bound ligand during transport (Chaptal *et al*, 2011). In $PepT_{St}$, peptide binding is likely to involve the conserved tyrosine residues, Tyr29 (H1) and Tyr68 (H2) from the N-terminal bundle, as these residues have important roles in determining binding affinity. Bound peptides may also interact with Glu400(H10), as suggested by Meredith and colleagues for PepT1 (Meredith *et al*, 2000; Xu *et al*, 2009) and by Jensen *et al*, for the *E. coli* POT transporter yjdL (Jensen *et al*, 2011). We predict that closure of the extracellular gate is facilitated by the formation of conserved salt bridge interactions between Arg53 (H1)–Glu312 (H7) and Arg33 (H1)–Glu300 (H7), although the latter is more conserved and important. Transition to the occluded state is likely to occur following the substantial

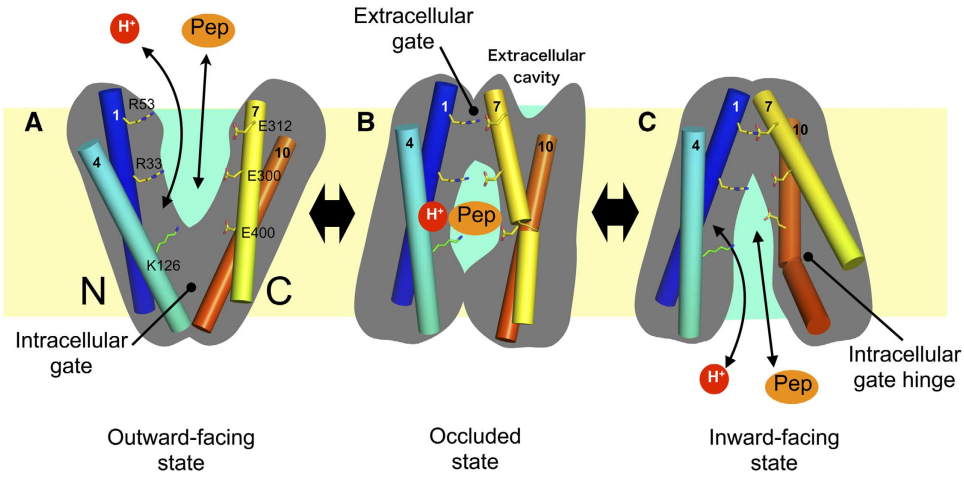

Figure 5 A model for proton-driven peptide symport by $PepT_{St}$. (**A**) $PepT_{St}$ adopts an outward facing state, here modelled on the outward facing fucose permease structure (PDB: 3O7Q). This state is characterized by the packing of helices H4, H5 with H10, H11 that form the intracellular gate and is potentially stabilized through a salt bridge interaction between K126 and E400 as discussed. Peptide (Pep) and proton (H^+) bind from the extracellular side of the membrane with important roles for the N-terminal ExxERFxYY motif on H1 and K126 in H4. (**B**) Binding results in closure of the extracellular gate to form the occluded state, here modelled on the occluded structure of $PepT_{So}$ (PDB: 2XUT). This conformation is characterized by the packing of helices H7, H8 against H1, H2 at the extracellular side of the binding site, assisted through the formation of the salt bridge interactions between R53-E312 and R33-E300. Binding of both peptide and proton is also likely to disrupt the proposed interaction between K126 and E400, thereby facilitating release of the intracellular gate. In the occluded state, an additional extracellular cavity may also form in the C-terminal domain following closure of the extracellular gate, as observed in the occluded $PepT_{So}$ structure. (**C**) Transition to the inward facing state, modelled on the inward facing $PepT_{St}$ structure (PDB: 4APS) occurs in part through a localized hinge-like movement in helices H10, H11 that results in release of the intracellular gate, allowing exit of proton and peptide into the interior of the cell.

inter-helical movement within the C-terminal half of the transporter, potentially resulting in the formation of an extracellular cavity, as observed in the structure of $PepT_{So}$ (Newstead *et al*, 2011). Closure of the extracellular gate is likely to weaken the proposed Lys126–Glu400 salt bridge forming part of the intracellular gate, in preparation for opening. To complete the cycle, the transporter must adopt an inward facing state that is likely to resemble the $PepT_{St}$ structure, with the central cavity accessible to the interior of the cell to release the bound peptide and proton (Figure 5C). Our analysis of the $PepT_{St}$ structure and comparison with the occluded $PepT_{So}$ conformation suggests that this occurs as a result of localized hinge-like bending in helices H10 and H11 at the conserved pivot points formed by Gly407 and Trp427. This is likely to occur in parallel with the movement of helix H7, consistent with our earlier suggestion that helices H7, H11 and H12 operate as a functional sub-bundle during transport (Newstead, 2011). To complete the transport cycle, the transporter must recycle back through an empty occluded state. Although precise mechanistic details remain to be determined, our model suggests that reorientation would require the re-pairing of the Lys126–Glu400 salt bridge between H4 and H10 at an early stage.

Dynamic salt bridge networks, such as we have suggested above for $PepT_{St}$ are important within many secondary active transporters for orchestrating structural re-arrangements during transport (Boudker and Verdon, 2010). The prominent role proposed for salt bridges in our model of peptide transport draws interesting parallels with similar models for LacY (Radestock and Forrest, 2011) and GlpT (Law *et al*, 2008), which invoke analogous cycles of salt bridge breakage and re-pairing during transport. In particular, within GlpT, salt bridge interactions between helices H1, H7 and H8 are observed and predicted to re-arrange upon substrate binding, whereas in LacY Kaback and colleagues propose an interaction between helices H8 and H10, involving a salt bridge between Glu269 and His322, that facilitates substrate binding (He and Kaback, 1997). A comparable interaction is observed in our structure of $PepT_{St}$ between Asn328 (H8) and Glu400 (H10). Clearly, specific interactions will differ between individual MFS transporters. With respect to peptide transport in particular, however, our model provides valuable new insight that facilitates a broader understanding of peptide transport within the POT family and provides further evidence that commonalities in mechanism are evident between evolutionarily distinct members of the MFS.

Materials and methods

Protein expression and purification

$PepT_{St}$ was identified as suitable for structural studies by fluorescence-based pre-crystallization screening and stability analysis (Sonoda *et al*, 2011). The gene encoding $PepT_{St}$ (Uniprot identifier Q5M4H8) was amplified from *Streptococcus thermophilus* strain LMG18311 genomic DNA and cloned into a C-terminal GFP fusion expression vector (Drew *et al*, 2006). Wild-type and mutant $PepT_{St}$ were purified to homogeneity using standard IMAC protocols in n-dodecyl-β-D-maltopyranoside (DDM) detergent as described previously (Newstead *et al*, 2011; Supplementary data). The protein was concentrated to 7 mg ml^{-1} for crystallization and stored at −80°C.

Crystallization and structure determination

Crystals of $PepT_{St}$ were initially obtained in the MemGold crystallization screen (Newstead *et al*, 2008; Molecular Dimensions Ltd, UK) and optimized to 26% PEG 400, 0.1 M MES (2-(*N*-morpholino)ethanesulphonic acid), pH 6.50, 0.03 M Magnesium Chloride and 1 mM Cadmium Chloride using the hanging drop vapour diffusion technique at 19°C. For cryoprotection, the

crystals were transferred to a solution containing 36–40% PEG 400, before being flash cooled in liquid nitrogen. The crystals always showed strong anisotropic diffraction, with the best crystals diffracting X-rays to Bragg spacing's of 3.3 Å in the strongest direction. Initial phases were calculated using MIRAS using two mercury-derivatized crystals combined with a seleno-L-methionine data set (Table I; Supplementary data). Data were collected on beamlines IO2, IO3 and IO4 at the Diamond Light Source Ltd, UK. The higher resolution native data were collected on IO2, processed and scaled using mosflm (Leslie and Powell, 2007) and aimless (Evans, 2011), whereas the heavy atom and lower resolution native data were processed by the XIA2 (Winter, 2009) pipeline to XDS (Kabsch, 2010). The space group was determined to be $P2_12_12_1$ with two molecules in the asymmetric unit. Two mercury sites were initially located manually using RSPS (Knight, 2000) with their positions further refined and initial phases calculated using SHARP with solvent flattening in SOLOMON (Abrahams and Leslie, 1996). The resulting experimental maps were of sufficient quality to see all 14 helices from each of the two molecules. Further improvement in map quality was obtained following cross crystal averaging in DMMulti (as described in Pedersen *et al*, 2010) between the mercury (MMC), selenium (Se) and the isomorphous 4 Å resolution native data (Table I).

Model building and refinement

The model was built into experimental maps calculated from SHARP and DMMulti, using O (Jones *et al*, 1991). The partial models were further cycled back into SOLOMON to improve the initial solvent envelope used for the solvent flipping procedure. The amino-acid side chains were then built using the selenium and mercury sites to determine the correct register. Refinement of the model was carried out in BUSTER (Blanc *et al*, 2004) against the highest resolution data set and using strict non-crystallographic symmetry restraints. Refinement was improved by anisotropic truncation of the structure factors (Strong *et al*, 2006) along the A and C axes to 3.6 Å, with the B axis kept at 3.3 Å. To increase the contribution of the high-resolution terms in the resulting 2mFo-DFc electron density maps, a B-factor sharpening term was introduced during map calculation in FFT of between -50 and -80 Å^2. Model validation was carried out using the Molprobity server (Davis *et al*, 2004). Images were prepared using PyMol (Schrodinger LLC, 2010).

Membrane reconstitution

Purified $PepT_{St}$ protein was exchanged into 50 mM KPi, 150 mM KCl, 0.3% DM (Anatrace, USA), pH 7.0 using a 10/300 superdex S200 gel filtration column (GE Healthcare, UK), prior to reconstitution. Liposomes were prepared from acetone-ether washed *E. coli* lipids and egg yolk L-α-phosphatidylcholine (Avanti Polar Lipids, USA) in a ratio of 3:1 (wt/wt) as described previously (Fang *et al*, 2000). Proteoliposomes, prepared at protein-to-lipid ratio of 1:40 (wt/wt), were formed through rapid dilution into 50 mM potassium phosphate, pH 7.0. Following ultracentrifugation at 4°C for 3 h at 130 000 *g*, the proteoliposomes were re-suspended to a final concentration of 4 mg ml^{-1} and subjected to five freeze-thaw cycles prior to storage at -80°C.

Transport assays

For proton-driven uptake assays, artificially imposed potassium ion diffusion potentials were generated as previously described (Foucaud and Poolman, 1992). This system uses the established $\Delta\Psi$ electrical potential across the liposome bilayer (interior negative; approximately -100 mV) to drive H^+ and peptide uptake. Proteoliposomes were thawed, centrifuged at 90 000 *g* for 30 min at 4°C and re-suspended in 20 mM Potassium Phosphate, pH 6.50, 100 mM Potassium Acetate, 2 mM Magnesium Sulphate, followed by 11 cycles of extrusion through a 400nm polycarbonate filter to obtain small unilamellar vesicles of relatively homogenous size (Knol *et al*, 1996). Proteoliposomes were subsequently diluted 1:50 (v/v) into external buffer containing 20 mM NaPIPES (piperazine-*N*,*N*′-bis(2-ethanesulphonic acid)), pH 6.0, 2 mM magnesium sulphate with 10 μM valinomycin and ^{3}H labelled peptides at varying concentrations. Uptake of ^{3}H peptides was assayed at 25°C as described in Supplementary data. Diluting aliquots into 1.5 ml of ice-cold 0.1 M lithium chloride stopped the reaction. Proteoliposomes were collected onto 0.22 μm nitrocellulose filters and washed under vacuum with excess 0.1 M lithium chloride prior to scintillation counting. The ^{3}H signal was converted to molar concentrations of peptide using standard curves for each substrate. For ligand-driven counterflow transport (Kaback *et al*, 2001), proteoliposomes were re-suspended in 50 mM Potassium Phosphate, pH 6.5, 2 mM Magnesium Sulphate and 10 mM Ala-Ala. Transport was started following a 1:50 (v/v) dilution into 50 mM Potassium Phosphate, pH 6.50, 2 mM Magnesium Sulphate containing 5 μM ^{3}H Ala-Ala.

Accession codes

The atomic coordinates have been deposited in the Protein Data Bank with accession code 4APS.

Supplementary data

Supplementary data are available at *The EMBO Journal* Online (http://www.embojournal.org).

Acknowledgements

This research was funded primarily through the Medical Research Council (MRC) Career Development Award grant G0900399 to SN with important contributions from the Wellcome Trust via grant 062164/Z/00/Z to SI and Wellcome Trust Structural Biology DPhil studentship to NS. DD is funded through the Royal Society university research fellowship scheme. We also thank the beamline staff at the Diamond Light Source Ltd, UK (IO2, IO3 and IO4) and the support team at the Research Complex at Harwell, UK.

Author contributions: SN and DD devised and implemented stability-based screening of PepT homologues. NS, DD, JK and SN expressed, purified and crystallized $PepT_{St}$. SN and AD solved the heavy atom sub-structure, built the model and refined the structure. NS and SN designed, performed and interpreted the transport assay data. PWF performed and analysed the molecular dynamics calculations. SN wrote the paper with assistance from NS, DD, AD, PWF and SI.

Conflict of interest

The authors declare that they have no conflict of interest.

References

Abrahams JP, Leslie AGW (1996) Methods used in the structure determination of bovine mitochondrial F1 ATPase. *Acta Crystallogr D Biol Crystallogr* **52:** 30–42

Abramson J, Smirnova I, Kasho V, Verner G, Kaback HR, Iwata S (2003) Structure and mechanism of the lactose permease of Escherichia coli. *Science* **301:** 610–615

Anderson CMH, Thwaites DT (2010) Hijacking solute carriers for proton-coupled drug transport. *Physiology* **25:** 364–377

Biegel A, Knutter I, Hartrodt B, Gebauer S, Theis S, Luckner P, Kottra G, Rastetter M, Zebisch K, Thondorf I, Daniel H, Neubert K, Brandsch M (2006) The renal type H+/peptide symporter PEPT2: structure-affinity relationships. *Amino Acids* **31:** 137–156

Blanc E, Roversi P, Vonrhein C, Flensburg C, Lea SM, Bricogne G (2004) Refinement of severely incomplete structures with maximum likelihood in BUSTER-TNT. *Acta Crystallogr D Biol Crystallogr* **60:** 2210–2221

Bolger MB, Haworth IS, Yeung AK, Ann D, Grafenstein von H, Hamm-Alvarez S, Okamoto CT, Kim KJ, Basu SK, Wu S, Lee VH (1998) Structure, function, and molecular modeling approaches to the study of the intestinal dipeptide transporter PepT1. *J Pharm Sci* **87:** 1286–1291

Boudker O, Verdon G (2010) Structural perspectives on secondary active transporters. *Trends Pharmacol Sci* **31:** 418–426

Brandsch M (2009) Transport of drugs by proton-coupled peptide transporters: pearls and pitfalls. *Expert Opin Drug Metab Toxicol* **5:** 889–905

Chaptal V, Kwon S, Sawaya MR, Guan L, Kaback HR, Abramson J (2011) Crystal structure of lactose permease in complex with an

affinity inactivator yields unique insight into sugar recognition. *Proc Natl Acad Sci USA* **108:** 9361–9366

Dang S, Sun L, Huang Y, Lu F, Liu Y, Gong H, Wang J, Yan N (2010) Structure of a fucose transporter in an outward-open conformation. *Nature* **467:** 734–738

Daniel H, Kottra G (2004) The proton oligopeptide cotransporter family SLC15 in physiology and pharmacology. *Pflugers Arch* **447:** 610–618

Daniel H, Rubio-Aliaga I (2003) An update on renal peptide transporters. *Am J Physiol Renal Physiol* **284:** F885–F892

Daniel H, Spanier B, Kottra G, Weitz D (2006) From bacteria to man: archaic proton-dependent peptide transporters at work. *Physiology* **21:** 93–102

Davis IW, Murray LW, Richardson JS, Richardson DC (2004) MOLPROBITY: structure validation and all-atom contact analysis for nucleic acids and their complexes. *Nucleic Acids Res* **32:** W615–W619

Döring F, Dorn D, Bachfischer U, Amasheh S, Herget M, Daniel H (1996) Functional analysis of a chimeric mammalian peptide transporter derived from the intestinal and renal isoforms *J Physiol* **497**(Pt 3): 773–779

Döring F, Martini C, Walter J, Daniel H (2002) Importance of a small N-terminal region in mammalian peptide transporters for substrate affinity and function. *J Membr Biol* **186:** 55–62

Drew D, Lerch M, Kunji E, Slotboom D, de Gier J (2006) Optimization of membrane protein overexpression and purification using GFP fusions. *Nat Methods* **3:** 303–313

Eddy E, Wood C, Miller J, Wilson G (1995) A comparison of the affinities of dipeptides and antibiotics for the di-/tripeptide transporter in Caco-2 cells. *Int J Pharm* **115:** 79–86

Ernst HA, Pham A, Hald H, Kastrup JS, Rahman M, Mirza O (2009) Ligand binding analyses of the putative peptide transporter YjdL from E. coli display a significant selectivity towards dipeptides. *Biochem Biophys Res Commun* **389:** 112–116

Evans PR (2011) An introduction to data reduction: space-group determination, scaling and intensity statistics. *Acta Crystallogr D Biol Crystallogr* **67:** 282–292

Fang G, Konings WN, Poolman B (2000) Kinetics and substrate specificity of membrane-reconstituted peptide transporter DtpT of Lactococcus lactis. *J Bacteriol* **182:** 2530–2535

Fei YJ, Kanai Y, Nussberger S, Ganapathy V, Leibach FH, Romero MF, Singh SK, Boron WF, Hediger MA (1994) Expression cloning of a mammalian proton-coupled oligopeptide transporter. *Nature* **368:** 563–566

Fei YJ, Liu JC, Fujita T, Liang R, Ganapathy V, Leibach FH (1998) Identification of a potential substrate binding domain in the mammalian peptide transporters PEPT1 and PEPT2 using PEPT1-PEPT2 and PEPT2-PEPT1 chimeras. *Biochem Biophys Res Commun* **246:** 39–44

Forrest LR, Krämer R, Ziegler C (2011) The structural basis of secondary active transport mechanisms. *Biochim Biophys Acta* **1807:** 167–188

Foucaud C, Poolman B (1992) Lactose transport system of Streptococcus thermophilus. Functional reconstitution of the protein and characterization of the kinetic mechanism of transport. *J Biol Chem* **267:** 22087–22094

Harder D, Stolz J, Casagrande F, Obrdlik P, Weitz D, Fotiadis D, Daniel H (2008) DtpB (YhiP) and DtpA (TppB, YdgR) are prototypical proton-dependent peptide transporters of Escherichia coli. *FEBS J* **275:** 3290–3298

He MM, Kaback HR (1997) Interaction between residues Glu269 (helix VIII) and His322 (helix X) of the lactose permease of Escherichia coli is essential for substrate binding. *Biochemistry* **36:** 13688–13692

Hirai T, Heymann JAW, Shi D, Sarker R, Maloney PC, Subramaniam S (2002) Three-dimensional structure of a bacterial oxalate transporter. *Nat Struct Biol* **9:** 597–600

Huang Y, Lemieux MJ, Song J, Auer M, Wang D-N (2003) Structure and mechanism of the glycerol-3-phosphate transporter from Escherichia coli. *Science* **301:** 616–620

Jensen JM, Ernst HA, Wang X, Hald H, Ditta AC, Ismat F, Rahman M, Mirza O (2011) Functional investigation of conserved membrane-embedded glutamate residues in the proton-coupled peptide transporter YjdL. *Protein Pept Lett* **19:** 282–287

Jones TA, Zou JY, Cowan SW, Kjeldgaard M (1991) Improved methods for building protein models in electron density maps and the location of errors in these models. *Acta Crystallogr A* **47**(Pt 2): 110–119

Kaback HR, Sahin-Tóth M, Weinglass AB (2001) The kamikaze approach to membrane transport. *Nat Rev Mol Cell Biol* **2:** 610–620

Kaback HR, Smirnova I, Kasho V, Nie Y, Zhou Y (2011) The alternating access transport mechanism in LacY. *J Membr Biol* **239:** 85–93

Kabsch W (2010) XDS. *Acta Crystallogr D Biol Crystallogr* **66:** 125–132

Knight SD (2000) RSPS version 4.0: a semi-interactive vector-search program for solving heavy-atom derivatives. *Acta Crystallogr D Biol Crystallogr* **56:** 42–47

Knol J, Veenhoff L, Liang WJ, Henderson PJ, Leblanc G, Poolman B (1996) Unidirectional reconstitution into detergent-destabilized liposomes of the purified lactose transport system of Streptococcus thermophilus. *J Biol Chem* **271:** 15358–15366

Law CJ, Maloney PC, Wang D-N (2008) Ins and outs of major facilitator superfamily antiporters. *Annu Rev Microbiol* **62:** 289–305

Leibach FH, Ganapathy V (1996) Peptide transporters in the intestine and the kidney. *Annu Rev Nutr* **16:** 99–119

Lemieux MJ, Huang Y, Wang D-N (2004) Glycerol-3-phosphate transporter of Escherichia coli: structure, function and regulation. *Res Microbiol* **155:** 623–629

Leslie AGW, Powell HR (2007) *NATO Science Series II: Mathematics, Physics and Chemistry*, Read RJ, Sussman JL (eds). Dordrecht, Netherlands: Springer

Liang R, Fei YJ, Prasad PD, Ramamoorthy S, Han H, Yang-Feng TL, Hediger MA, Ganapathy V, Leibach FH (1995) Human intestinal H+/peptide cotransporter. Cloning, functional expression, and chromosomal localization. *J Biol Chem* **270:** 6456–6463

Luckner P, Brandsch M (2005) Interaction of 31 beta-lactam antibiotics with the H+/peptide symporter PEPT2: analysis of affinity constants and comparison with PEPT1. *Eur J Pharm Biopharm* **59:** 17–24

Malle E, Zhou H, Neuhold J, Spitzenberger B, Klepsch F, Pollak T, Bergner O, Ecker GF, Stolt-Bergner PC (2011) Random mutagenesis of the prokaryotic peptide transporter YdgR identifies potential periplasmic gating residues. *J Biol Chem* **286:** 23121–23131

Matthews DM (1975) Intestinal absorption of peptides. *Physiol Rev* **55:** 537–608

Matthews DM (1991) *Protein Absorption: Development and Present State of the Subject*. New York: Wiley-Liss Publishers

Meredith D, Temple CS, Guha N, Sword CJ, Boyd CA, Collier ID, Morgan KM, Bailey PD (2000) Modified amino acids and peptides as substrates for the intestinal peptide transporter PepT1. *Eur J Biochem* **267:** 3723–3728

Newstead S (2011) Towards a structural understanding of drug and peptide transport within the proton-dependent oligopeptide transporter (POT) family. *Biochem Soc Trans* **39:** 1353–1358

Newstead S, Drew D, Cameron AD, Postis VLG, Xia X, Fowler PW, Ingram JC, Carpenter EP, Sansom MSP, Mcpherson MJ, Baldwin SA, Iwata S (2011) Crystal structure of a prokaryotic homologue of the mammalian oligopeptide-proton symporters, PepT1 and PepT2. *EMBO J* **30:** 417–426

Newstead S, Ferrandon S, Iwata S (2008) Rationalizing alpha-helical membrane protein crystallization. *Protein Sci* **17:** 466–472

Pao SS, Paulsen IT, Saier MH (1998) Major facilitator superfamily. *Microbiol Mol Biol Rev* **62:** 1–34

Pedersen BP, Morth JP, Nissen P (2010) Structure determination using poorly diffracting membrane-protein crystals: the H+-ATPase and Na+, K+-ATPase case history. *Acta Crystallogr D Biol Crystallogr* **66:** 309–313

Pieri M, Gan C, Bailey P, Meredith D (2009) The transmembrane tyrosines Y56, Y91 and Y167 play important roles in determining the affinity and transport rate of the rabbit proton-coupled peptide transporter PepT1. *Int J Biochem Cell Biol* **41:** 2204–2213

Radestock S, Forrest LR (2011) The alternating-access mechanism of MFS transporters arises from inverted-topology repeats. *J Mol Biol* **407:** 698–715

Sala-Rabanal M, Loo DDF, Hirayama BA, Wright EM (2008) Molecular mechanism of dipeptide and drug transport by the human renal H+/oligopeptide cotransporter hPEPT2. *Am J Physiol Renal Physiol* **294:** F1422–F1432

Schrodinger LLC (2010) The PyMOL Molecular Graphics System, Version 1.3r1

Smirnova I, Kasho V, Kaback HR (2011) Lactose permease and the alternating access mechanism. *Biochemistry* **50:** 9684–9693

Sonoda Y, Newstead S, Hu N-J, Alguel Y, Nji E, Beis K, Yashiro S, Lee C, Leung J, Cameron AD, Byrne B, Iwata S, Drew D (2011) Benchmarking membrane protein detergent stability for improving throughput of high-resolution X-ray structures. *Structure* **19:** 17–25

Steinhardt HJ, Adibi SA (1986) Kinetics and characteristics of absorption from an equimolar mixture of 12 glycyl-dipeptides in human jejunum. *Gastroenterology* **90:** 577–582

Strong M, Sawaya MR, Wang S, Phillips M, Cascio D, Eisenberg D (2006) Toward the structural genomics of complexes: crystal structure of a PE/PPE protein complex from Mycobacterium tuberculosis. *Proc Natl Acad Sci USA* **103:** 8060–8065

Weitz D, Harder D, Casagrande F, Fotiadis D, Obrdlik P, Kelety B, Daniel H (2007) Functional and structural characterization of a prokaryotic peptide transporter with features similar to mammalian PEPT1. *J Biol Chem* **282:** 2832–2839

Winter G (2009) xia2: an expert system for macromolecular crystallography data reduction. *J Appl Crystallogr* **43:** 186–190

Xu L, Haworth IS, Kulkarni AA, Bolger MB, Davies DL (2009) Mutagenesis and cysteine scanning of transmembrane domain 10 of the human dipeptide transporter. *Pharm Res* **26:** 2358–2366

Yin Y, He X, Szewczyk P, Nguyen T, Chang G (2006) Structure of the multidrug transporter EmrD from Escherichia coli. *Science* **312:** 741–744